2014 IEEE International Conference on Robotics & Automation (ICRA)
Hong Kong Convention and Exhibition Center
May 31 - June 7, 2014. Hong Kong, China

Energetic Effects of Reaction Wheel Actuation on Underactuated Biped Robot Walking

Travis L. Brown and James P. Schmiedeler

***Abstract*— Inertial actuators, such as reaction wheels, have the potential to improve the stability and robustness of bipedal robots. While the stabilizing capabilities of reaction wheels follow naturally from physical laws, the effects on walking efficiency are less clear. This work examines those effects by comparing energy-optimal periodic gaits for a variety of under-actuated, five-link planar biped configurations. When energy consumption is normalized by total mass, bipeds equipped with reaction wheels have decreased walking cost compared to unequipped bipeds of the same mass across a wide range of conditions. At speeds equal to or higher than the optimal walking speed, reaction wheels can reduce walking cost by approximately 8%. When walking with large step lengths, reaction wheels decrease walking costs by more than 20% and allow bipeds to take longer steps. Efficiency improvements scale with the momentum capacity of the reaction wheel, but saturate for particularly large reaction wheels.**

I. INTRODUCTION

Walking robots have been a focus of research for decades due to their potential to navigate rough terrain and operate in spaces optimized for human locomotion. Many walking robots use powerful ankles and large, flat feet to provide stabilizing torques to the robot. This ankle torque strategy is one of several used by humans to maintain balance [1], but has limitations. For example, the foot size limits the maximum stabilizing torque, and sophisticated sensing and control are required to adapt to terrain irregularity [2].

These and other limitations motivate use of another human strategy, accelerating the limbs or torso to exert similar stabilizing torques [3]. Due to the mathematical complexity of this approach, body parts are often lumped together and modeled as a single rotating reaction wheel [3]–[7]. When the robot is in contact with the ground, accelerating this virtual reaction wheel to generate torque is mathematically equivalent to using ankle actuators [8]. Because the limbs and body have restrictive joint limits (often less than a full rotation), though, torques can only be exerted for a short time and must be reversed shortly thereafter to prevent joint limit violation [6]. Additionally, the prescribed motion of the joints may conflict with preexisting motion goals.

One alternative is to include dedicated inertial actuators such as reaction wheels or control moment gyroscopes (CMGs), which are free of joint limits and don't interfere with task space goals. Such actuators are commonly used for satellite attitude control, have been suggested for space-based robots [9], and have been studied as stabilization aids for humans [10]. In terms of legged robots, walking biped robots have been stabilized in experiment with reaction wheels [11] and in simulation with CMGs [12]. Mayer et al. examined the stability properties of a reaction wheel-equipped biped [13] and introduced a mechanical brake that facilitated dynamic maneuvers by rapidly stopping the spinning wheel to exert large torques [14].

T. L. Brown and J. P. Schmiedeler are with the Department of Aerospace and Mechanical Engineering, University of Notre Dame, Notre Dame, IN, 46556, USA. {Email: tbrown14@nd.edu and schmiedeler.4@nd.edu}

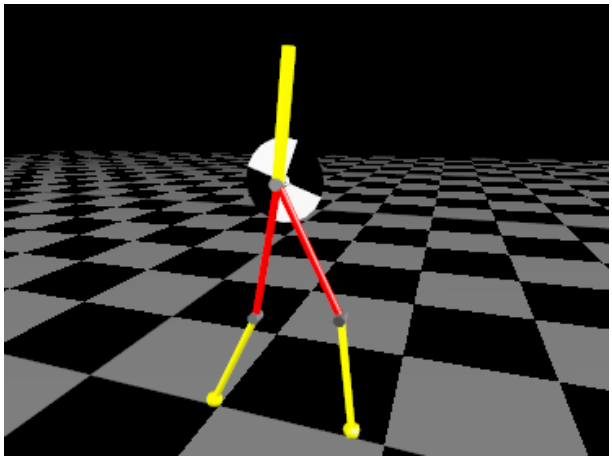

Fig. 1: Five-link planar biped consisting of a torso (yellow), 2 thighs (red), 2 shanks (yellow), and a reaction wheel (black and white) connected to the torso coincident with the hip

While the stabilizing effects of reaction wheels and CMGs have been studied, their effect on periodic walking gait has not been well established. In terms of efficiency, the additional mass associated with inertial actuators would likely increase the energetic cost of walking. These actuators, however, may expand the design space of achievable gaits, thereby mitigating the rise in energetic cost by making more efficient gaits possible. The extent of this effect is not trivial to determine, nor is it clear how the effect is influenced by the mass and efficiency of the inertial stabilizer itself. This work addresses these questions by generating energy-optimal periodic gaits for a model (shown in Fig. 1) of an existing five-link planar biped robot to which various reaction wheel stabilizer (RWS) systems are added. Attributes of these optimal gaits are compared to quantify the energetic effects of using the different RWS systems in steady state walking.

II. METHODS

Most approaches to generate optimal, dynamically feasible motion trajectories for walking robots differ in the way the problem is formulated to leverage existing optimization algorithms. Forward dynamics approaches [15]–[18]

optimize over the space of control inputs and use time integration to generate the state trajectory. Inverse dynamics approaches [19], [20] optimize state trajectories and use inverse dynamics to generate corresponding control inputs. This work uses Posa and Tedrake's [21] approach to simultaneously optimize over the state and control trajectories. All gradients are computed analytically, and the resulting gradient matrix is sparse, so the problem can be efficiently solved using large scale gradient-based optimization.

A. System Model

The system model is based on the planar, five-link, underactuated biped ERNIE [22] in Fig. 2. ERNIE is treated as a simple mechanical system with equations of motion expressed in terms of generalized coordinates q and velocities $\dot{q}$.

$$M(\mathbf{q})\ddot{\mathbf{q}} + C(\dot{\mathbf{q}}, \mathbf{q})\dot{\mathbf{q}} + G(\mathbf{q}) = B(\mathbf{q})\mathbf{u} + R(\mathbf{q})\lambda, \quad (1)$$

where M is the mass matrix, C is the Coriolis matrix, G is the gravity vector, B is the matrix relating control inputs (u) to generalized forces, and R is the reaction matrix relating contact forces (λ) to generalized forces. For the five-link model, the generalized coordinates are the Cartesian coordinates of the hip, torso angle, thigh angles, shank angles, and angle of the reaction wheel. The existing ERNIE hardware has four joint motors, two at the hip and one at each knee. A fifth motor is added to the model to connect the reaction wheel to the torso. Since the reaction wheel torques are independent of its location on the torso, the RWS is mounted at the hip to avoid additional gravitational torques on the body. The reaction wheel is assumed to have all mass ideally distributed at its radius.

Six contact variables were included, two to model hard-stops at the knees that prevent hyperextension and four to represent the normal and tangential components of the contact forces on the feet. Model parameters for the biped and reaction wheel are listed in Table I, with biped parameters taken from [23]. All joint motor parameters were taken from published values for the Maxon 136212 motor with a 91:1 gear reduction, which matches the current ERNIE hardware. The same motor was used to model the reaction wheel actuator since the demands on it are anticipated to be similar, but the gear reduction was halved to be consistent with lower backdrive losses and higher regenerative efficiency.

B. Optimization Formulation

As in Posa and Tedrake [21], system trajectories are encoded by a time-series of N waypoints consisting of generalized coordinates, generalized velocities, control inputs, and contact forces.

$$X = \big[\{\mathbf{q_1}, \dot{\mathbf{q}}_\mathbf{1}, \mathbf{u_1}, \lambda_\mathbf{1}\}, \{\mathbf{q_2}, \dot{\mathbf{q}}_\mathbf{2}, \mathbf{u_2}, \lambda_\mathbf{2}\}, \cdots, \{\mathbf{q_N}, \dot{\mathbf{q}}_\mathbf{N}, \mathbf{u_N}, \lambda_\mathbf{N}\}, h\big], \quad (2)$$

where waypoints are separated by time steps of length h. The equations of motion in (1) can be rewritten as a nonlinear constraint equation using a finite difference approximation of the second derivative of the generalized coordinates.

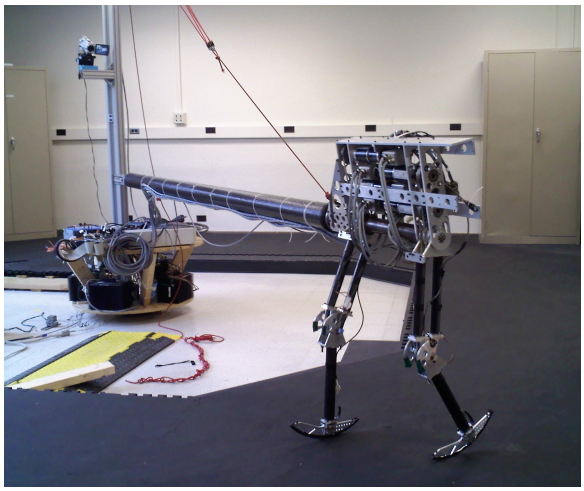

Fig. 2: Planar biped ERNIE, the physical system on which the five-link biped model is based.

$$\mathbf{q_i} - \mathbf{q}_{i-1} - h\dot{\mathbf{q}}_i = 0 \quad (3)$$

$$M_i[\dot{\mathbf{q}}_i - \dot{\mathbf{q}}_{i-1}] + h[C_i\dot{\mathbf{q}}_i + G_i(\mathbf{q_i}) - B_i\mathbf{u_i} + R_i\lambda_\mathbf{i}] = 0. \quad (4)$$

In addition to dynamic motion constraints, a set of contact constraints must also be enforced.

$$\lambda_{i,z} \geq 0 \quad (5)$$

$$\mu\lambda_{i,z} - \lambda_{i,x} \geq 0 \quad (6)$$

$$\lambda_{1,z} + \lambda_{2,z} - \lambda_{min} \geq 0 \quad (7)$$

$$\Phi(\mathbf{q}_i) \geq 0 \quad (8)$$

$$\Phi(\mathbf{q}_i) \cdot \lambda_{i,z} = 0 \quad (9)$$

$$R_i^T\dot{\mathbf{q}}_i \cdot \lambda_{i,z} = 0, \quad (10)$$

where Φ is the contact distance function, $R_i^T\dot{\mathbf{q}}_\mathbf{i}$ is the velocity in contact space, and $\lambda_{i,x}$ and $\lambda_{i,z}$ represent contact forces parallel and normal to the ground, respectively. Equation 6 enforces a friction cone constraint, where μ is the friction coefficient of the contact surface. The non-penetration constraint in Eq. 8 requires the distance to contact points to be positive. The nonlinear complementarity condition in Eq. 9 requires contact forces to be non-zero only when contact points are touching. The no-slip condition in Eq. 10 enforces zero relative motion when contact forces are non-zero. To maintain a minimum swing foot ground clearance so as to avoid unintentional ground contacts resulting from joint tracking errors and measurement noise, (8) is modified as

$$\Phi(\mathbf{q}_i) > C(\mathbf{q}_i, t), \quad (11)$$

where $C(q_i, t)$ is a clipped and scaled time-based parabolic clearance function ranging from zero at the beginning/end of each step to C_{max} at mid-stance. See Fig. 3.

Further constraints on the states, velocities, joint angles, joint rates, and motor torques were also applied (Table I). Maximum joint rates and motor torques were chosen to

TABLE I: Modeling and optimization parameters

Model parameter	Units	Link	Value
Mass	kg	body	13.6
		thigh	1.5
		shank	1.0
Length	m	body	0.28
		thigh	0.36
		shank	0.36
Mass center	m	body	0.14
		thigh	0.13
		shank	0.12
Inertia	kg m^2	body	0.09
		thigh	0.02
		shank	0.02

Optimization parameters	Symbol	Units	Value
Waypoints	N	-	60
Gearhead ratio	N_r	-	91:1
RWS radius	-	cm	10
Friction Coefficient	μ	-	0.9
Max. ground clearance	C_{max}	m	0.1
Min. vertical g.r.f.	λ_{min}	N	10
Min. knee flexion	K_{flex}	deg	15
Step Length Limits	-	m	[0.1, 2.0]
Hip Height Limits	-	m	[0.43, 0.72]
Thigh Angle Limits	-	rad	$\pm\pi/2$
Shank Angle Limits	-	rad	$\pm\pi/2$
Body Angle Limits	-	rad	± 0.1
Joint rate limits	-	rpm	± 120
RWS rate limits	-	rpm	± 240
Joint torque limits		N-m	± 40
RWS torque limits		N-m	± 20

match current ERNIE hardware. The hip height was constrained to be above 60% of total leg length to prevent excessive crouching, and knee and hip joints were constrained to avoid interference. To represent a well regulated upper body posture, the torso angle was constrained to ± 0.1 rad. A minimum knee flexion angle K_{flex} was used to better reflect the bent-knee stance common on many robots lacking hardstops [22]. To ensure forward motion, the difference between x_h (horizontal hip position) for the first and last waypoint is constrained to be greater than a minimum step-length. For periodicity, the first and last waypoints are constrained to be identical (excluding x_h), and variables corresponding to the left and right legs are switched to allow optimization of only a half step.

There is no consensus in the literature as to the most appropriate energetic cost function. Two common elements of such cost functions are torque squared and mechanical power. Electrical energy consumption, the sum of the integrals of the electrical power consumption over the trajectory for each motor, was used in this work since it is a first order approximation of energetic cost for typical robot hardware and includes both common elements. Assuming a resistive, non-inductive DC motor model, the instantaneous power

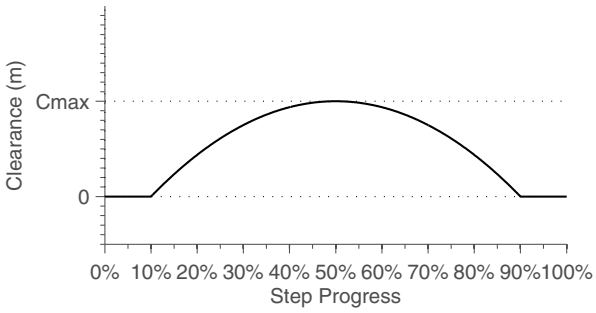

Fig. 3: Ground clearance constraint to prevent unintended foot contact with the ground

(P_m) at each waypoint is a combination of resistive losses in the armature and mechanical work.

$$P_m = (\frac{\tau}{N_r k_t})^2 R_a + (\frac{\tau}{k_t})\omega k_v, \tag{12}$$

where τ is the motor torque, ω is the motor velocity, k_t and k_v are the motor's torque and voltage constants, and N_r is the gear reduction. To account for friction and electrical losses in the motor controller, an efficiency coefficient η is added to the mechanical work term. To simulate different levels of regenerative efficiency on each motor, η is changed according to the sign of the motor work.

$$\eta = \begin{cases} \eta_{pos} & \text{if } \omega\tau > 0, \\ \eta_{neg} & \text{if } \omega\tau < 0, \end{cases} \tag{13}$$

where η_{pos} is the positive work efficiency and η_{neg} is the regenerative efficiency of negative work. The gradient discontinuity introduced at $\omega\tau = 0$ is avoided by adding a third order polynomial spline function that smoothly transitions between η_{pos} and η_{neg} near $\omega\tau = 0$. The total energy cost of a trajectory can be approximated by

$$E(X) = h\sum_{i=2}^{N} \frac{R_a}{(k_t N_r)^2}\mathbf{u_i}\cdot\mathbf{u_i} + \eta\mathbf{u_i}(\frac{B^T\dot{\mathbf{q}}_{i-1} + B^T\dot{\mathbf{q}}_i}{2}), \tag{14}$$

where ω is calculated using the trapezoidal rule between pairs of consecutive joint-space velocities. Because most of the joints are heavily geared and consequently suffer significant backdrive losses, regenerative efficiency on the limb joints was 0%. Since the reaction wheel can be viewed as an energy storage mechanism as well as a stabilization system, more efficient hardware is likely justifiable. To explore this possibility, efficiencies of 0%, 50%, and 100% were used.

The optimization problem can be stated as a search for the trajectory requiring the smallest energy per distance traveled.

$$\begin{aligned} \underset{X}{\text{minimize}} \quad & \frac{E(X)}{d_s(X)} \\ \text{subject to} \quad & \text{Equations } (3)-(11), \end{aligned}$$

where d_s is the step length of the trajectory.

C. Optimization method

This formulation requires a large number of waypoints to avoid errors from the finite difference approximation, yielding hundreds of optimization variables. Both the constraint equations and cost function, however, have analytical first derivatives, so gradient-based optimization is efficient. Additionally, constraints act across at most two waypoints, resulting in a sparse system that can be efficiently solved by large-scale gradient-based optimization packages like SNOPT, which was used here.

The primary disadvantage of this approach is its dependency on the seed trajectory due to the existence of local minima. To increase the likelihood of converging to a globally optimal trajectory, a continuation method approach to seeding was pursued in which each optimization in a series was seeded with the results of the previous optimization. When the optimization converged to a trajectory that was significantly different from trajectories prior trajectories, several other similar seed trajectories were tried and the lowest cost result was recorded.

III. RESULTS

To compare systems of different sizes and weights, key quantities of interest can be nondimensionalized. Walking speeds are normalized by the square root of the product of gravity and the total leg length ($\frac{v}{\sqrt{gl}}$), yielding what is sometimes known as the Froude number or specific speed. Step lengths are normalized by leg length. Energetic cost is expressed as the specific cost of transport, equal to energy divided by the product of step length, total mass, and gravity $c_{et} = (\frac{E(X)}{mgd_s})$. Since this efficiency metric is normalized by mass, the additional mass of an RWS tends to cancel out the energetic cost of carrying it onboard. This work assumes that the enhanced disturbance rejection capabilities provided by an RWS justify the extra payload, so the focus here is on using the RWS to improve efficiency in undisturbed gait as well.

A. Effects of Mass Distribution and Walking Constraints

To compare RWS- and non-RWS-equipped bipeds, the energetic cost of adding mass to the torso is established. The mass effects were highly dependent on knee flexion and ground clearance constraints, as determined by optimizing gaits for four different constraint configurations across a range of body masses. Figure 4 shows c_{et}at the optimal walking speed and step length for these four configurations, with increasing body mass indicated by an increasing ratio of body mass to leg mass since leg mass is constant. The first three configurations use the ground clearance constraint in Fig. 3, while the fourth does not, so it approximates a compass gait.

The first configuration imposes a minimum stance knee flexion of 15^o and exhibits a strong increase in cost of transport as body mass increases, likely due to the larger static torques which have a quadratic effect on energy consumption. The third and fourth cases have no stance knee flexion constraint, so the stance knees can be locked at

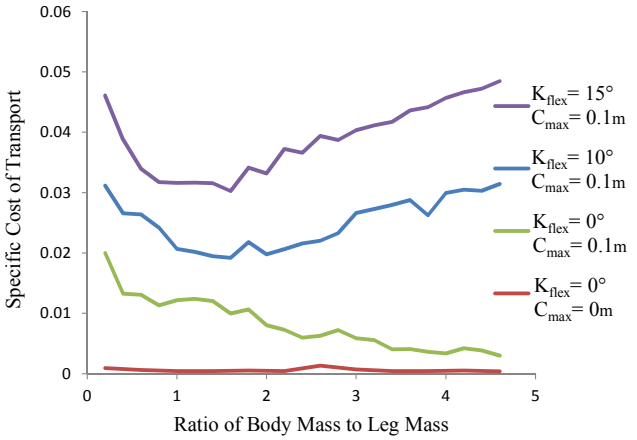

Fig. 4: Minimum walking cost for the base (non-RWS) system with four different constraint configurations

the hardstops, meaning that repositioning the legs accounts for most of the energy. In both cases, c_{et} decreases with increased mass because of the normalization by mass. The second case with a 10^o minimum knee flexion constraint falls between the first and third cases. From these results, it is clear that the energy penalty for carrying the mass of an RWS is significantly larger for bipeds that must maintain knee flexion throughout stance than for bipeds that can walk in a human-like, straight-legged manner. This highlights one of the benefits of inertial actuators; unlike ankle joints, they can be moved to the body where, assuming straight-legged gaits are possible, added mass does not significantly affect walking efficiency. The subsequent results use the ground clearance constraint and the 15^o stance knee flexion constraint. To avoid sensitivity to mass effects, bipeds without an RWS are loaded with an equivalent mass.

B. Effect of Reaction Wheels on Efficiency

Optimizations were performed across a range of walking speeds for four cases of the biped model, three equipped with a 10kg RWS with different levels of regenerative efficiency and one loaded with a 10kg point mass at the hip. Figure 5 shows the reduction in c_{et} for the RWS-equipped bipeds as a percent of the baseline for the biped with just the point mass. RWS efficiency has a major effect on the potential improvement. For 0% and 50% regeneration, the reduction in c_{et} is approximately 2% over almost the entire range of speeds examined. With 100% regeneration, the cost reduction is significantly higher, ranging from 4-12%. This difference suggests that efficiency improvements are primarily due to the RWS efficiently storing and releasing large amounts of energy at specific points in the gait. Only minor improvements likely come from the added control authority provided by the extra degree of freedom. Figure 6 shows the state trajectory and control torques for a biped equipped with a 100% regenerative RWS and walking at a normalized speed of 0.18. The most notable behavior is a strong positive control torque on the RWS shortly before

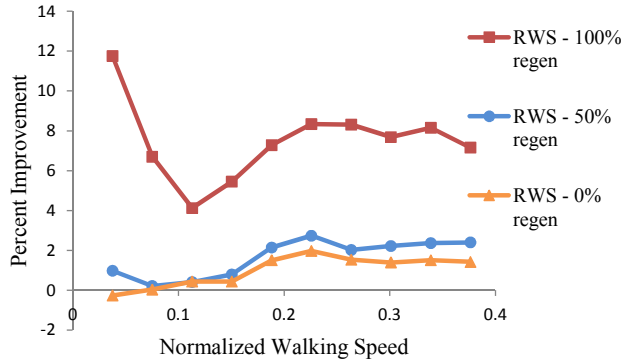

Fig. 5: Percent improvement in specific cost of transport resulting from RWS use compared to the baseline non-RWS system. The RWS benefits increase with increasing walking speed regardless of regenerative efficiency.

touchdown at the end of the gait. This likely serves to redirect the motion of the center of mass, similar to toe-off behavior in ankle-equipped bipeds.

Since foot placement requirements may prevent a biped from walking at its preferred step length, the energetic effects of an RWS at non-optimal step lengths are important. To examine these effects, the four configurations were evaluated at normalized step lengths ranging from 0.1 to 1. Figure 7 shows the resulting c_{et} curves. In all cases, walking cost increases significantly as the step length increases. For the non-RWS-equipped biped, the optimization fails to return dynamically feasible, constraint-satisfying gaits when step length reaches 1.25. Conversely, for RWS-equipped bipeds, an exaggerated RWS utilization strategy allows the biped to extend its range of feasible step lengths and decrease energy consumption by more than 20% at longer step lengths. The reaction wheel builds momentum during a step and then transfers it to the body by exerting torque on the body both before and after touchdown. This compensates for lost momentum and pushes the biped forward, allowing it to recover from its heavily splayed posture. The reaction wheel is then recharged, and the cycle repeats. Again, there are parallels with the effects of toe-off. See the attached video or visit `http://ame-robotics.nd.edu/LAB/Robots/Walking.php` to see a demonstration of this behavior.

C. Reaction Wheel Sizing

A series of optimizations was performed to determine the effects of reaction wheel mass on energy savings. Figure 8 shows the improvement percentages for four different reaction wheel masses with 100% regenerative efficiency. The results fail to show a correlation between reaction wheel mass and efficiency improvement for reaction wheel masses above 2.5 kg. Control torque and velocity profiles show that peak reaction wheel velocity decreases with increasing wheel mass, but the control torque does not. This suggests that there is a limit to the amount of efficiency that can be gained

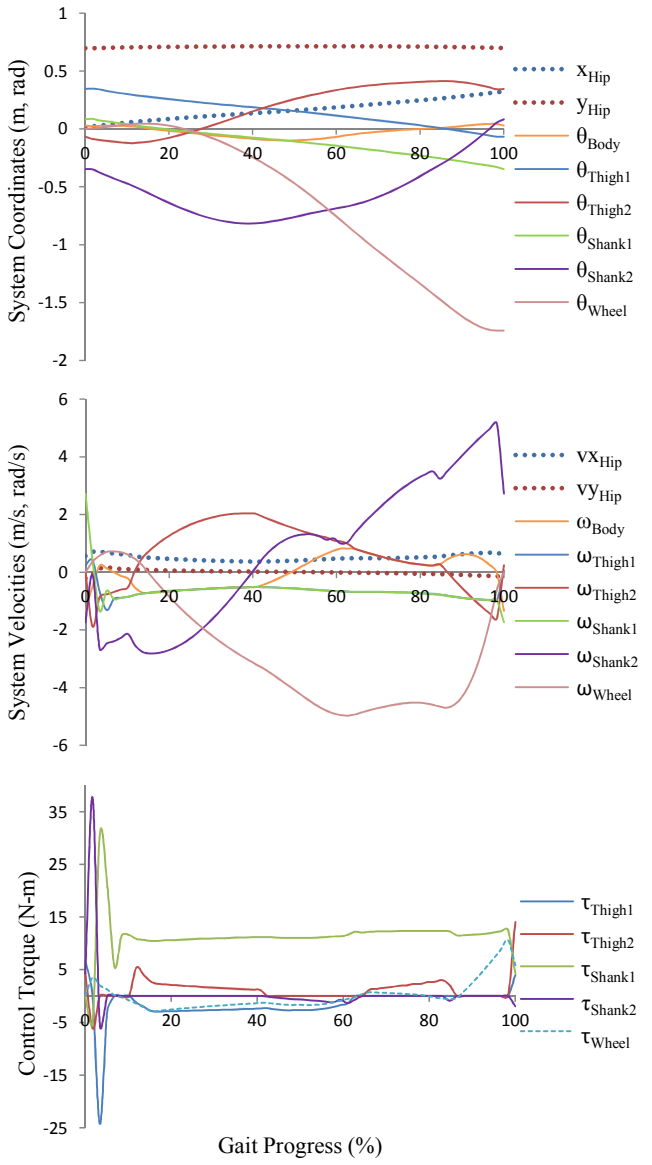

Fig. 6: Positions, velocities, and control torques for an RWS-equipped biped walking at a normalized speed of 0.18. Transfer of support occurs at the beginning of the gait, after which leg #1 is the stance leg.

through momentum storage and return strategies. At a mass of 1 kg, the speed of the reaction wheel saturates during the gait, so efficiency improvement is limited.

IV. CONCLUSION

This work explored the energetic effects of reaction wheel stabilizer (RWS) systems on underactuated, planar biped walking. When energy consumption is normalized by total biped mass, these systems offer efficiency improvements over a static payload of equal size. The results show that an RWS is most beneficial when operating at above-optimal speeds and step lengths. At the optimal normalized walking speed, a reaction wheel as small as 12% of total robot mass with

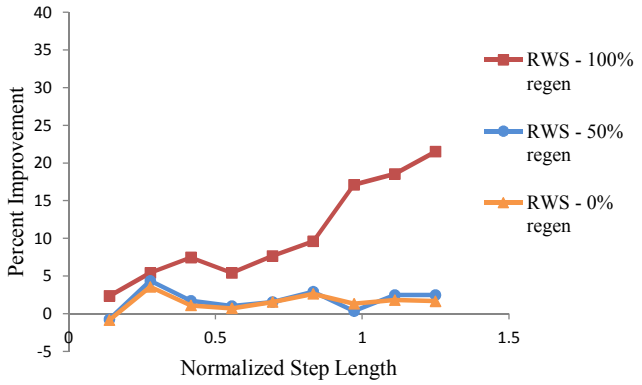

Fig. 7: Walking cost reduction for three RWS-equipped biped configurations evaluated through a range of step lengths. Improvements are most pronounced at longer step lengths.

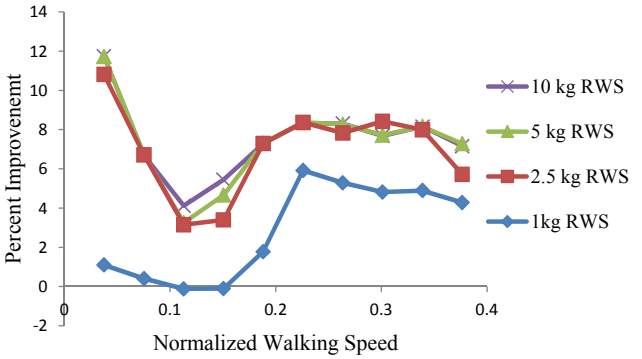

Fig. 8: Comparison of the improvement in specific cost of transport possible with four different reaction wheel configurations. Larger reaction wheels lead to better efficiency, but the effect saturates at larger wheel sizes.

100% regenerative efficiency can reduce energy consumption by up to 8%. These improvements, however, are highly dependent on regeneration efficiency. With no regeneration, the improvement drops to 1-2%. Efficiency improvement is largely independent of reaction wheel mass for large reaction wheels, but is negatively effected if reaction wheel size is too small. The most significant benefit of an RWS system was found at large step lengths, when an RWS can potentially reduce walking cost by more than 20% and expand the range of feasible gaits. This may be energetically beneficial in terrain where foot placement is highly constrained. Overall, the efficiency improvements possible with reaction wheels are modest and alone would likely not justify the extra cost and complexity of their inclusion. However, when considered together with their unique stabilization capabilities, the potential for increased efficiency strengthens the argument for using dedicated inertial actuators in walking robots.

REFERENCES

[1] D. A. Winter, "Human balance and posture control during standing and walking," *Gait & Posture*, vol. 3, no. 4, pp. 193–214, 1995.

[2] S. Hyon & G. Cheng, "Simultaneous adaptation to rough terrain & unknown external forces for biped humanoids," in *7th IEEE-RAS Int. Conference on Humanoid Robots*, 2007, pp. 19–26.

[3] A. Goswami, "Kinematic & dynamic analogies between planar biped robots and the reaction mass pendulum (RMP) model," in *8th IEEE-RAS Int. Conference on Humanoid Robots*, 2008, pp. 182–188.

[4] J. Pratt, J. Carff, S. Drakunov, & A. Goswami, "Capture point: A step toward humanoid push recovery," in *6th IEEE-RAS Int. Conference on Humanoid Robots*, 2006, pp. 200–207.

[5] Y. Wei, B. Gang, & W. Zuwen, "Balance recovery for humanoid robot in the presence of unknown external push," in *IEEE Int. Conference on Mechatronics & Automation*, 2009, pp. 1928–1933.

[6] B. Stephens, "Humanoid push recovery," in *7th IEEE-RAS Int. Conference on Humanoid Robots*, 2007, pp. 589–595.

[7] T. Komura, H. Leung, S. Kudoh, & J. Kuffner, "A feedback controller for biped humanoids that can counteract large perturbations during gait," in *IEEE Int. Conference on Robotics & Automation*, 2005, pp. 1989–1995.

[8] J. E. Pratt, "Exploiting inherent robustness & natural dynamics in the control of bipedal walking robots," Ph.D. dissertation, Massachusetts Institute of Technology, 2000.

[9] M. Carpenter & M. Peck, "Dynamics of a high-agility, low-power imaging payload," *IEEE Transactions on Robotics*, vol. 24, no. 3, pp. 666–675, 2008.

[10] D. Li & H. Vallery, "Gyroscopic assistance for human balance," in *12th IEEE Int. Workshop on Advanced Motion Control*, 2012, pp. 1–6.

[11] K. Tsujita & K. Tsuchiya, "An experimental study on motion control of a biped locomotion machine using reaction wheels," in *Experimental Robotics IV*, O. Khatib & J. Salisbury, Eds. Springer, 1997, vol. 223, pp. 558–565.

[12] T. Wong & Y. Hung, "Stabilization of biped dynamic walking using gyroscopic couple," in *IEEE Int. Joint Symposia on Intelligence & Systems*, 1996, pp. 102–108.

[13] N. M. Mayer, K. Masui, M. Browne, & M. Asada, "Gyro stabilized biped walking," in *IEEE/RSJ Int. Conference on Intelligent Robots & Systems*, 2006, pp. 1422–1427.

[14] N. Mayer, F. Farkas, & M. Asada, "Balanced walking & rapid movements in a biped robot by using a symmetric rotor & a brake," in *IEEE Int. Conference on Mechatronics & Automation*, vol. 1, 2005, pp. 345–350.

[15] L. Roussel, C. C. de Wit, & A. Goswami, "Generation of energy optimal complete gait cycles for biped robots," in *IEEE Int. Conference on Robotics & Automation*, 1998, pp. 2036–2041.

[16] M. Srinivasan & A. Ruina, "Computer optimization of a minimal biped model discovers walking & running," *Nature*, vol. 439, no. 7072, pp. 72–75, 2006.

[17] F. C. Anderson & M. G. Pandy, "Dynamic optimization of human walking." *Journal of Biomechanical Engineering*, vol. 123, no. 5, pp. 381–390, 2001.

[18] G. Schultz & K. Mombaur, "Modeling & optimal control of human-like running," *IEEE/ASME Transactions on Mechatronics*, vol. 15, no. 5, pp. 783–792, 2010.

[19] H. J. Kim, Q. Wang, S. Rahmatalla, C. C. Swan, J. S. Arora, K. Abdel-Malek, and J. G. Assouline, "Dynamic motion planning of 3D human locomotion using gradient-based optimization," *Journal of Biomechanical Engineering*, vol. 130, no. 3, 031002, 2008.

[20] T. Erez & E. Todorov, "Trajectory optimization for domains with contacts using inverse dynamics," in *IEEE/RSJ Int. Conference on Intelligent Robots & Systems*, 2012, pp. 4914–4919.

[21] M. Posa & R. Tedrake, "Direct trajectory optimization of rigid body dynamical systems through contact," in *Algorithmic Foundations of Robotics X*, E. Frazzoli, T. Lozano-Perez, N. Roy, & D. Rus, Eds. Springer, 2013, vol. 86, pp. 527–542.

[22] T. Yang, E. R. Westervelt, J. P. Schmiedeler, & R. A. Bockbrader, "Design & control of a planar bipedal robot ernie with parallel knee compliance," *Autonomous Robots*, vol. 25, no. 4, pp. 317–330, 2008.

[23] T. Yang, E. R. Westervelt, A. Serrani, & J. P Schmiedeler, "A framework for the control of stable aperiodic walking in underactuated planar bipeds," *Autonomous Robots*, vol. 27, pp. 277–290, 2009.